PHYSICAL REVIEW C **96**, 034617 (2017)

Nuclear-matter radius studies from ^{58}Ni(α,α) experiments at the GSI Experimental Storage Ring with the EXL facility

J. C. Zamora,[1,*] T. Aumann,[1,2] S. Bagchi,[2,3] S. Bönig,[1] M. Csatlós,[4] I. Dillmann,[2,5] C. Dimopoulou,[2] P. Egelhof,[2] V. Eremin,[6] T. Furuno,[7] H. Geissel,[2,5] R. Gernhäuser,[8] M. N. Harakeh,[3] A.-L. Hartig,[1] S. Ilieva,[1] N. Kalantar-Nayestanaki,[3] O. Kiselev,[2] H. Kollmus,[2] C. Kozhuharov,[2] A. Krasznahorkay,[4] Th. Kröll,[1] M. Kuilman,[3] S. Litvinov,[2] Yu. A. Litvinov,[2] M. Mahjour-Shafiei,[3,9] M. Mutterer,[2] D. Nagae,[10] M. A. Najafi,[3] C. Nociforo,[2] F. Nolden,[2] U. Popp,[2] C. Rigollet,[3] S. Roy,[3] C. Scheidenberger,[2,5] M. von Schmid,[1] M. Steck,[2] B. Streicher,[2] L. Stuhl,[4] M. Thürauf,[1] T. Uesaka,[11] H. Weick,[2] J. S. Winfield,[2] D. Winters,[2] P. J. Woods,[12] T. Yamaguchi,[13] K. Yue,[1,2,14] and J. Zenihiro[11]

[1]*Institut für Kernphysik, Technische Universität Darmstadt, Darmstadt, Germany*
[2]*GSI Helmholtzzentrum für Schwerionenforschung GmbH, Darmstadt, Germany*
[3]*KVI-CART, University of Groningen, Groningen, The Netherlands*
[4]*Institute for Nuclear Research, MTA-Atomki, Debrecen, Hungary*
[5]*Physikalisches Institut, Justus-Liebig-Universität Giessen, Giessen, Germany*
[6]*Ioffe Physical-Technical Institute, St. Petersburg, Russia*
[7]*Division of Physics and Astronomy, Kyoto University, Kyoto, Japan*
[8]*Physik-Department E12, Technische Universität München, München, Germany*
[9]*Department of Physics, University of Tehran, Tehran, Iran*
[10]*Department of Physics, University of Tsukuba, Tsukuba, Japan*
[11]*RIKEN Nishina Center, Wako, Saitama, Japan*
[12]*Institute for Particle and Nuclear Physics, University of Edinburgh, Edinburgh, United Kingdom*
[13]*Department of Physics, Saitama University, Sakura-ku, Saitama, Japan*
[14]*Institute of Modern Physics, Chinese Academy of Sciences, Lanzhou, China*

(Received 22 June 2017; published 22 September 2017)

A novel method for measuring nuclear reactions in inverse kinematics with stored ion beams was successfully used to extract the nuclear-matter radius of ^{58}Ni. The experiment was performed at the experimental heavy-ion storage ring at the GSI facility using a stored ^{58}Ni beam at energies of 100 and 150 MeV/u and an internal helium gas-jet target. Elastically scattered α-recoils at low momentum transfers were measured with an in-ring detector system compatible with ultrahigh vacuum. Experimental angular distributions were fitted using density-dependent optical model potentials within the eikonal approximation. This permitted the extraction of the point-matter root-mean-square radius of ^{58}Ni with an average value of 3.70(7) fm. Results from this work are in good agreement with several experiments performed in the past in normal kinematics. This pioneering experiment demonstrates a major breakthrough towards future investigations with far-from-stability stored beams using the present technique.

DOI: 10.1103/PhysRevC.96.034617

I. INTRODUCTION

Scattering of electromagnetic and hadronic probes off nuclei have brought new discoveries and essential information on bulk properties and structure of nuclei over the past several years. Since the pioneering experiments of Rutherford [1] using scattering of α particles and Hofstadter [2] using scattering of electrons, this type of experiments became a major tool to measure the nuclear size and its radial distribution. In particular, experiments using electron scattering (which interact with nucleons primarily through the relatively weak electromagnetic interaction) are quite useful to obtain the charge density distribution of nuclei. Complementary to this technique, hadron scattering is sensitive to the nuclear force, and that makes it an excellent probe to extract the matter-density distribution of nuclei. For instance, nucleon and light-ion scattering experiments have been extensively used in normal-kinematics experiments to measure the matter radii of a wide range of nuclei [3,4]. This technique also led to the discovery of extended neutron distributions (or neutron skin) and halos in exotic nuclei [5–8]. One interesting feature in these nuclei is that their charge and matter distributions can differ significantly, which is an effect arising from the existence of neutron skins. Systematic studies of nuclear-matter radii along isotopic chains covering a large domain of N/Z ratios, including neutron-deficient and neutron-rich nuclei, are essential for understanding properties of the nuclear matter under extreme conditions (e.g., in astrophysical scenarios like neutron stars). In particular, thicknesses of neutron skins are of great importance to determine the asymmetry term of the equation of state (EoS) of the nuclear matter [9,10].

In the past, experiments performed in normal kinematics using proton or light-ion (e.g., d or α) beams, at intermediate and high energies, were employed to extract the matter radius of only stable nuclei. Usually, high-resolution spectrographs permitted to measure angular distributions of elastic scattering at forward angles in the center-of-mass system ($\theta_{\text{c.m.}}$), which is the most sensitive range of the cross section to obtain

*zamora@nscl.msu.edu

the nuclear radius. However, this technique is limited to the study stable nuclei due the impossibility to produce targets of short-lived nuclei. Therefore, novel techniques have been developed using radioactive beams in inverse-kinematics experiments. For example, the use of a first generation of active targets permitted to deduce successfully the nuclear-matter distribution of light exotic-nuclei [5–8]. Nevertheless, such experiments were limited due to the angular resolution and detection sensitivity for the recoiling particles at very forward angles in center-of-mass frame.

In this work, a new method, which permits high-resolution measurements of direct reactions in inverse kinematics at very low momentum transfer, is used. This method is the stored-beam technique, which is the basis of the EXL (exotic nuclei studied with light-ion induced reactions in storage rings) project [11,12] that is presently being operated at the existing experimental heavy-ion storage ring (ESR) [13] at the GSI facility. This project is part of the program for nuclear structure, astrophysics, and reaction (NUSTAR) studies at the future facility for antiproton and ion research (FAIR) [11] under construction at GSI.

The novel method explained in this paper was successfully applied in a first in-ring nuclear reaction experiment with a stored radioactive ^{56}Ni beam, and it was recently reported in Ref. [14]. Also, a recent study of isoscalar giant resonances in a stored-beam experiment using inelastic α scattering was reported in Ref. [15]. In the present work, we use this versatile technique to investigate the nuclear-matter radius of a stored ^{58}Ni beam from elastically scattered α recoils measured simultaneously with the data reported in Ref. [15]. The experimental procedure is explained below.

II. EXPERIMENT

The present experiment was carried out at the heavy-ion storage ring ESR at the GSI facility [13]. The ESR has a circumference of about 108 m and a maximum magnetic rigidity of 10 Tm that allows to store ion beams (up to uranium with energies up to 560 MeV/u) delivered from the UNILAC-SIS18 accelerator complex. A ^{58}Ni beam was produced and accelerated up to the energy of 150 MeV/u and injected into the ESR. With each beam injection, about 10^8 particles were stored in the ring. Then, the ESR electron-cooler reduces the large emittance of the injected beam (in the order of 5π mm mrad) to less than 0.1π mm mrad, and at the same time, increases the momentum resolution of the beam ($\Delta p/p \leqslant 10^{-5}$ [16]). After cooling at injection energy, the stored beam can be decelerated to a constant lower energy by use of the magnets and rf system of the ESR. In this work, measurements with stored ^{58}Ni beam at the energies of 100 and 150 MeV/u are presented. At these energies the beam revolution frequencies in the ESR are about 1.2 and 1.4 MHz, respectively. Also, an internal gas-jet target system was used in this experiment [17]. This target consisted of a helium gas-jet, perpendicular to the beam direction, with a diameter of about 7 mm at the interaction zone with the cooled beam (σ value of less than 1 mm). This system was operated with a cryogenically cooled gas-source ($\sim$20 K) in order to improve the density of the gas target [18]. An average target density of 7×10^{12} part./cm^2 was achieved in the experiment. Nevertheless, this low target density was well compensated by the beam revolution frequency, which leads to a significant improvement in the luminosity. Luminosities of the order of 10^{25} to 10^{26} cm^{-2}s^{-1} were obtained in our measurements.

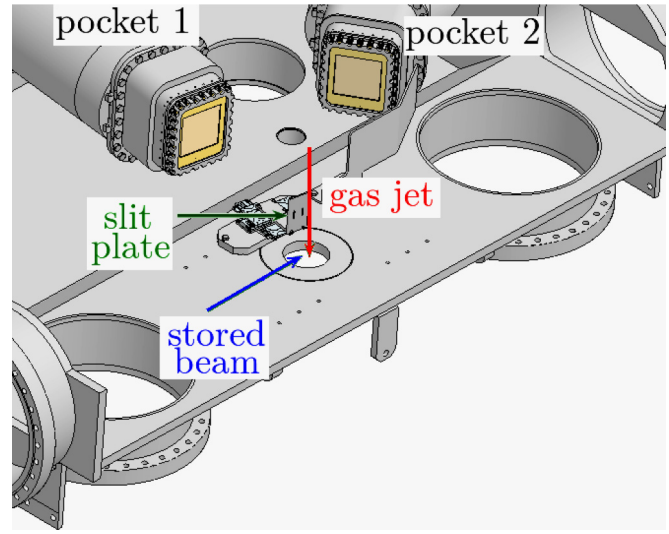

FIG. 1. Schematic illustration of the vacuum chamber installed in the ESR for the present experiment [19]. The stored beam interacts with the gas-jet target oriented perpendicular to the beam. The detectors were assembled at two internal pockets centered at 81° and 32°, with respect to the beam direction. A slit plate was installed in front of the pocket centered at 81° (pocket 1) in order to reduce the angular spread caused by the extension of the target.

As the main objective of this experiment was to measure recoils at very low momentum transfer, a detector setup mounted inside the ring was required. However, the vacuum needed for the ESR operation is in the ultrahigh vacuum (UHV) regime (in the order of 10^{-10} mbar or below) and at this level any type of outgassing material can significantly deteriorate the vacuum conditions. An additional requirement for our detector setup was to be resistant to temperatures up to 150°C, because a *bake-out* (at this temperature or higher) of the detector chamber for several days is essential for achieving UHV conditions in the ESR. In order to comply with these requirements, the detector array was installed in a vacuum chamber especially designed for compatibility with UHV and composed of two internal *pockets* covering the laboratory angular ranges of 74° to 89° and 27° to 37°, as illustrated in Fig. 1.

A DSSD (double-sided silicon strip detector) of 285 μm thickness, 64×64 mm^2 in area and with 128×64 orthogonally oriented strips was installed on the in-ring side of each pocket. This configuration permitted to separate the UHV of the ring from an auxiliary vacuum ($\sim 10^{-8}$ mbar) inside the pockets where all unbakeable and outgassing elements (e.g., connectors, cabling, etc.) were placed. Thus, the DSSDs were used as *active vacuum windows* for both recoil detection and to separate the two environments [19,20]. The pocket which was mounted in the angular range between 74° and 89°, named pocket 1, comprised also two Si(Li) detectors (which cannot be baked) of 6.5 mm thickness and an active

area of 100×56 mm^2 divided in eight quadratic pads with independent readout. These detectors were placed behind the DSSD with their respective cooling system (needed to cool the detectors during the baking procedure and also during operation) in a telescope configuration which allows detection of elastically scattered recoils in a wide energy range. Pocket 2, covering the angles from 27° to 37°, comprised a single DSSD for the detection of inelastically scattered recoils. Experimental results from measurements performed with this detector are reported in Ref. [15].

The angular resolution in this experiment was kinematically limited by the extension of the gas-jet target. A slit plate inside the chamber was included to reduce the acceptance and thus improve the angular resolution of the telescope of pocket 1 (down to 0.1° in the laboratory. system). An illustration of the slit plate installed in front of the gas jet (and parallel to the DSSD of pocket 1) can be seen in Fig. 1. The slit plate was mounted on two remote-controlled piezo stepper-motors, which were placed directly in the UHV. The construction enabled two-dimensional positioning of the slit aperture with a precision of below 5 μm. However, the improvement of the angular resolution comes at the cost of a significant reduction (about a factor five) in the count rate expected in the detectors of pocket 1. A Monte Carlo simulation using the toolkit GEANT4 [21] was performed to obtain the respective solid angle covered by each detector strip. Relative positions between the center of the target and the slit plate and DSSDs were corrected by fitting experimental spectra with GEANT4 simulations. Additionally, a correlation between DSSD pixels and spherical coordinates was derived from these simulations. This allows to calibrate the angular positions of each strip (or pixel) with respect to the target center.

III. RESULTS

As mentioned in the previous section, angular positions and kinetic energies of recoil particles were measured simultaneously by using DSSDs. The angular resolution achieved by using a slit plate permitted to identify kinematic lines of elastic scattering and excitation of a few low-lying states of ^{58}Ni. Figure 2 shows a two-dimensional (2D) scatter-plot measured in the experiment $^{58}\mathrm{Ni} + \alpha$ at 150 MeV/u. The x axis of the 2D plot, which originally corresponds to the number of the vertical strips of the detector, was transformed into polar angles by GEANT4 simulations with the corrected geometry of the setup. The most intense kinematic line, at the right side of the spectrum, corresponds to elastic scattering measurements at forward angles (down to 2°) in the center-of-mass system. Moreover, the excited states 2^+_1 (1.45 MeV) and 3^-_1 (4.47 MeV) of ^{58}Ni were also observed, and their kinematic lines are included in Fig. 2 for a better visualization.

The background contribution in these measurements is mainly produced by multiple scattering on the slit plate. Simulations and measurements without the slit plate demonstrate that the background component from residual-gas scattering and other types of nuclear reactions, like knockout, is small compared to scattering from the slit plate [22]. An average background distribution was deduced from the same experimental data by using vertical strips covering angles from

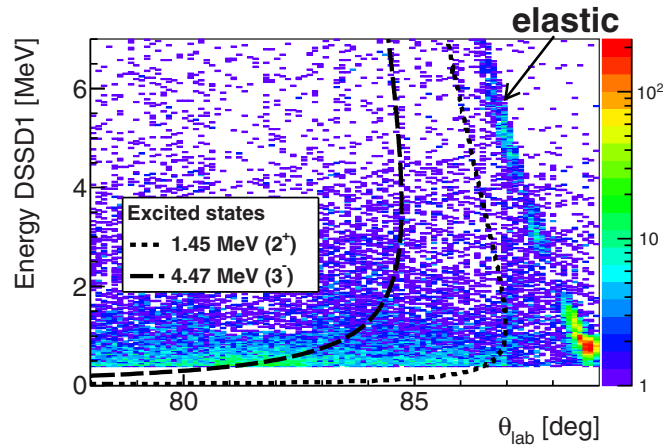

FIG. 2. Energy deposited by recoils in the vertical strips of DSSD1 (pocket 1) vs. laboratory polar angle corresponding to each strip. Elastic scattering can be observed at angles from 86° to 89°. Inelastic scattering reaction channels can also be observed and their kinematics are highlighted with the dashed lines.

74° to 82° which is a region dominated by background. As expected, the resulting average distribution is more significant at energies below 1 MeV and decreases quickly at higher energies. The background was then subtracted from the energy spectra of each vertical strip of DSSD1. This procedure was particularly important for reducing the statistical uncertainty around minima in the differential cross section for elastic scattering. However, given the small signal-to-background ratio around the kinematic lines, it was not possible to determine the angular distributions of inelastic scattering to the excited states. Elastic scattering angular distributions from the experiments at 100 and 150 MeV/u were extracted after their respective background subtraction. Figure 3 shows these angular distributions of the differential cross sections as ratios to the Rutherford cross sections. The laboratory angular range from 86° to 89° represents angles in the center-of-mass system between 2° and 8°. The angular resolution achieved in these measurements was about 0.2° in the center-of-mass system. For both incident energies, the cross section was measured around its first minimum, which is an angular region very sensitive to the nuclear size.

The present experimental data are well described with three different optical model potentials (OMP). The density-dependent Gaussian interaction and Woods-Saxon potential (DDG/WS) potential is a single folding of a density-dependent Gaussian interaction (range $t = 1.88$ fm) for the real part, and an imaginary Woods-Saxon potential [23]. This OMP has been successfully used for the description of α-particle scattering at low and intermediate energies [24]. A density-dependent scaling function is included in this interaction in order to reduce the strength in the interior of the folded potential while leaving the peripheral values unchanged. This is especially important for the description of the nuclear collisions at intermediate energies and at low momentum transfers. Parameters of this potential were obtained by fitting the experimental data using the program SFRESCO [25]. The fit values are presented in Table I.

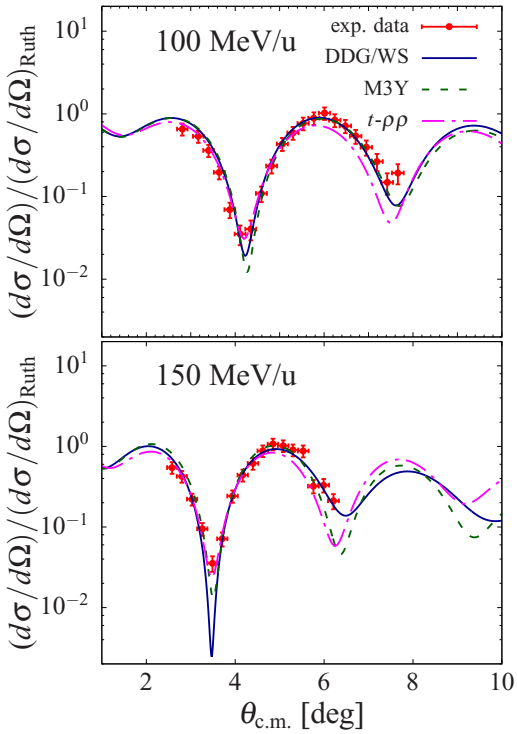

FIG. 3. Elastic scattering cross section of ^{58}Ni + α at 100 and 150 MeV/u. The differential cross section is presented as ratio to the Rutherford elastic scattering cross section. The experimental data was fitted using different optical model potentials (for details see text).

Another OMP employed in the analysis was a double-folding potential with the well-known M3Y interaction. The M3Y parametrization used for this work is the one explained in Ref. [26]. Similarly, this OMP has been widely and in general successfully used to analyze heavy-ion scattering. In particular, this potential leads to good results at intermediate and high energies in cases where the nuclear reactions are mostly peripheral [26,27]. With this double-folding interaction it is possible to create an OMP by applying the same form for both real and imaginary potentials. In this case, only potential depths are adjusted to fit the experimental data. The resulting potential depths for each data set (100 and 150 MeV/u) are listed in Table I.

In principle, the reaction cross section can be obtained from the previous OMP analysis in order to deduce the nuclear-matter radius. In this procedure, the absorption probability (obtained from the S matrix of the elastic scattering calculation) is fitted by assuming the soft-spheres approximation [28]. However, with a diffuse OMP (like in the present case) usually the nuclear surface and radius are overestimated [29,30]. Therefore, a method which involves a direct fit of a nuclear density parametrization to the experimental angular distribution would be preferred. This can be done in the optical limit of the Glauber theory with the microscopic t-$\rho\rho$ potential [31]. For nucleus-nucleus collisions this OMP has the form

$$U_{\rm opt}(\mathbf{r}) = \int \langle t_{NN}\rangle \rho_{\rm T}(\mathbf{r}-\mathbf{r}')\rho_{\rm B}(\mathbf{r}')d^3r', \qquad (1)$$

where $\rho_{\rm T}$ ($\rho_{\rm B}$) is the ground-state density of the target (beam) nucleus and $\langle t_{NN}\rangle$ is the isospin-averaged transition matrix element for nucleon-nucleon scattering at zero momentum transfer. In this work, the Glauber model analysis was applied in the zero-range approximation. In the past, this was proved to work well in the relativistic-energy region, but at intermediary energies the reaction cross section is usually underestimated [32]. The nucleon-nucleon scattering amplitude assumed for this analysis is the widely used parametrization [33,34]

$$f_{NN}(\mathbf{q}=0) = \frac{k_{NN}}{4\pi}\sigma_{NN}(\mathrm{i}+\alpha_{NN}), \qquad (2)$$

where k_{NN} is the nucleon momentum, σ_{NN} is the free nucleon-nucleon cross section, and α_{NN} is the ratio between the imaginary and the real part of the nucleon-nucleon scattering amplitude. σ_{NN}, α_{NN} are isospin-averaged parameters extracted from experimental p-p and p-n cross sections at different energies [33,34]. For instance, at the incident energy of 100 MeV/u the parameters $\sigma_{NN} = 52.9$ mb and $\alpha_{NN} = 1.43$ are employed, and at 150 MeV/u they are set to $\sigma_{NN} = 38.5$ mb and $\alpha_{NN} = 1.24$. Thus, the nucleon-nucleon interaction is fixed and the beam and target densities can then be optimized to fit the experimental angular distributions. This procedure is explained below.

TABLE I. Optical model potential parameters fitted to α elastic scattering on ^{58}Ni at 100 (data set A) and 150 MeV/u (data set B). The Coulomb radius was fixed as $r_{\rm C} = 1.2$ fm. All radii are given in the reduced form r_x, where $R_x = r_x A_{\rm T}^{1/3}$ and $A_{\rm T} = 58$.

Data set	OMP	$V_{\rm R}$ [MeV]	$W_{\rm I}$ [MeV]	$r_{\rm I}$ [fm]	$a_{\rm I}$ [fm]
A	M3Y	96.65	70.73	-	-
A	DDG/WS	111.49	40.59	1.39	0.69
B	M3Y	88.56	93.25	-	-
B	DDG/WS	91.46	39.52	1.20	1.19

A. Derivation of the nuclear-matter radius

The nuclear-matter radius of ^{58}Ni was obtained from a fit to the elastic scattering cross section using the t-$\rho\rho$ potential. As discussed above, an important ingredient of this model is the folding of projectile and target ground-state densities. The density of the target nucleus (^{4}He) used in this analysis is a Gaussian parametrization deduced from electron scattering experiments [35]

$$\rho_{\rm T}(r) = \rho_{\rm T}(0)\exp\left(-\frac{r^2}{c^2}\right) \qquad (3)$$

with $c = 1.37$ fm and a normalization factor $\rho_{\rm T}(0) = 4/(c\sqrt{\pi})^3$. This distribution was fixed during the analysis. In the case of ^{58}Ni, a two-parameters Fermi distribution was assumed:

$$\rho_{\rm P}(r) = \rho_{\rm P}(0)\frac{1}{1+\exp\left(\frac{r-R}{a}\right)}, \qquad (4)$$

where its half-density radius, R, and the diffuseness, a, were optimized to fit the experimental angular distribution.

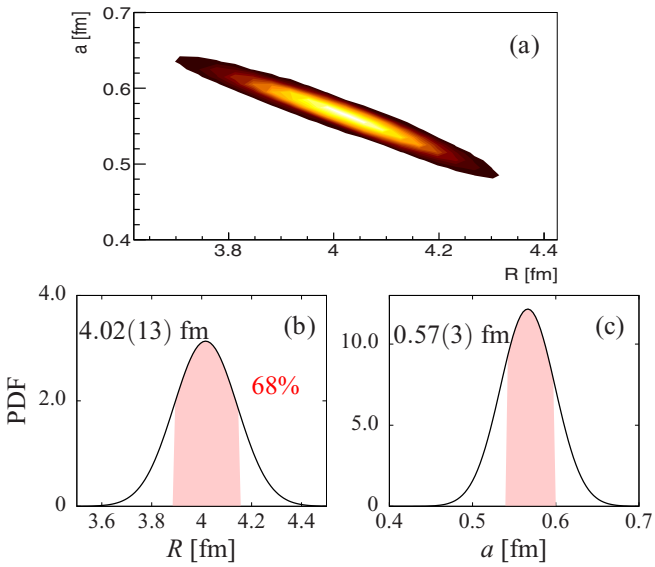

FIG. 4. (a) Probability density distribution obtained from a fit to the elastic scattering cross section using Eq. (4). At the bottom, one-dimensional PDFs [$p(x) = \int p(x,y)dy$] are shown for the half-density radius (b) and the diffuseness (c). The best fit values are obtained from each function assuming a 68% confidence interval.

Elastic scattering calculations for different sets of (R,a) were performed with the code DWEIKO [36]. For this work, it was necessary to implement minimization and density function routines into the code in order to fit the experimental data. The result of each calculation was stored in a two-dimensional χ^2 matrix. A probability density distribution was calculated by transforming each element of this matrix as [37]

$$P(R_i,a_j) \propto (\chi^2)^{(\nu/2-1)} \exp\left(-\frac{\chi^2}{2}\right), \tag{5}$$

where ν is the number of degrees of freedom. The best half-density radius and diffuseness were obtained from their respective probability density functions (PDF) assuming a confidence interval of 68%. Figure 4 shows a probability density distribution derived from the fit of the elastic scattering cross section data at 150 MeV/u. Shaded regions represent the confidence intervals taken in this analysis. The corresponding fit parameters can be found in Table II.

TABLE II. Results from the nuclear-matter density fit of ^{58}Ni. R and a are the half-density radius and diffuseness of a Fermi-shape density [Eq. (4)]. The rms radius: $\langle R_{\rm m}^2\rangle^{1/2}$ (total-matter distribution), $\langle r_{\rm m}^2\rangle^{1/2}$ (point-matter distribution), and $\langle r_n^2\rangle^{1/2}$ (point-neutron distribution). The neutron distribution is obtained by subtracting the (point-)matter distribution and the (point-)proton distribution calculated from Ref. [35]. All values are in fm.

Data set	R	a	$\langle R_{\rm m}^2\rangle^{1/2}$	$\langle r_{\rm m}^2\rangle^{1/2}$	$\langle r_n^2\rangle^{1/2}$
A	3.89(17)	0.62(4)	3.79(8)	3.71(9)	3.73(15)
B	4.02(14)	0.57(3)	3.76(7)	3.68(7)	3.69(13)
		Average	3.78(7)	3.70(7)	3.71(12)

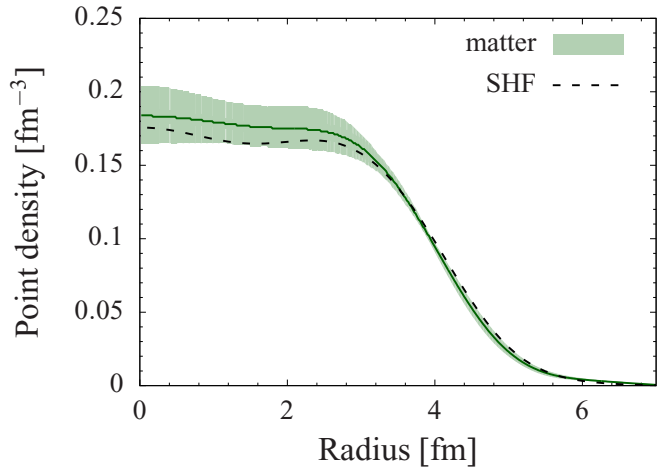

FIG. 5. Point-density distributions of ^{58}Ni deduced from the results of this work. The solid line is the result from the present experiment and the color band is its respective uncertainty. The point-matter density is compared with a Skyrme-Hartree-Fock calculation (SHF).

As can be seen in Fig. 3, this model is quite successful in describing the angular distributions at forward angles where the cross section is very sensitive to the nuclear-matter radius. The component at backward angles is more sensitive to the nuclear interior, and therefore the in-medium effects have more influence on the measured angular distributions. In this case, a renormalization of the free nucleon-nucleon parameters is required [31]. Nevertheless, a good description of the elastic scattering cross section around its first minimum is essential in order to extract the nuclear-matter radius. Often this radius is given in terms of the root-mean-square (rms) value

$$\langle R_{\rm m}^2\rangle^{1/2} = \left[\frac{\int_0^\infty \rho_{\rm P}(r) r^4 dr}{\int_0^\infty \rho_{\rm P}(r) r^2 dr}\right]^{1/2}, \tag{6}$$

where $\rho_{\rm P}(r)$ is the nuclear-density shape [Eq. (4)]. The rms radii of ^{58}Ni deduced from the experiments at 100 MeV/u and 150 MeV/u were 3.79(8) fm and 3.76(7) fm, respectively. These values are fully consistent with the ones reported from experiments of α scattering: 3.74(10) fm [3], and also from proton scattering: 3.74(5) fm [38]. However, we should note that the nuclear-matter density distribution extracted in this analysis also contains the finite size of the nucleons. This contribution can be unfolded by using phenomenological parametrizations for the nucleon form factors from Refs. [39,40]. Usually, this unfolded distribution is also called point-matter density, because nucleons are assumed as point-like particles. The ^{58}Ni point-matter density deduced from the present analysis is shown in Fig. 5, within its uncertainty band ($\pm 1\sigma$). For comparison, a Skyrme-Hartree-Fock (SHF) calculation is also plotted in the same figure. The SHF density was calculated with the code SKRYME_RPA [41], including the interaction SKO' [42]. As can be noted, these densities are in good agreement especially in the region of the nuclear surface. The rms point-radius of the SHF density is $\langle r_{\rm m}^2\rangle^{1/2} =$ 3.68 fm, which is also consistent with our experimental results presented in Table II and their average value 3.70(7) fm.

In order to deduce the radius of the neutron density and the neutron skin from this analysis, the charge density of ^{58}Ni (taken from electron scattering experiments, see Ref. [35]) was unfolded and subtracted from the present point-matter density. The average rms radius obtained from the point-neutron distributions was 3.71(12) fm. Also, the neutron skin thickness, defined as $\Delta r_{np} \equiv \langle r_n^2 \rangle^{1/2} - \langle r_p^2 \rangle^{1/2}$ (where $\langle r_p^2 \rangle^{1/2} = 3.68$ fm for ^{58}Ni [35]), was calculated in the present analysis with an average value of 0.03(12) fm. This result is consistent with the expectation for a symmetric nucleus ($\rho_p \approx \rho_n$) and also with literature values which range from -0.05 to 0.01 fm [43,44].

IV. SUMMARY

A novel technique for performing nuclear reaction experiments using stored ion beams and a UHV compatible detection system was successfully employed to study the nuclear-matter radius of ^{58}Ni. This unique technique allows to make measurements of recoil particles in inverse kinematics at very small momentum transfers, which is quite advantageous for the investigation of the nuclear bulk properties. Elastic α-scattering cross sections at forward angles in the center-of-mass frame were fitted by assuming a two-parameter Fermi density-distribution for ^{58}Ni. Results of the rms nuclear-matter and neutron radii of this work are in very good agreement with values reported from experiments performed in normal kinematics in the past using proton and alpha probes. This provides an important proof-of-principle towards prospective studies with far-from-stability radioactive beams with EXL. The technique is very versatile and also permits kinematically complete measurements of direct nuclear reactions with unstable nuclei. New experiments are already planned for continuation with the EXL program including an extended detector setup covering larger angular ranges for studies with unstable stored beams at GSI and in the future, at FAIR.

ACKNOWLEDGMENTS

We acknowledge technical support by A. Glazenborg-Kluttig, M. Lindemulder, P. Schakel, H. Timersma (KVI-CART, Groningen), J. Cavaco, G. May, L. Urban, and the accelerator staff (GSI, Darmstadt). This work was supported by German BMBF (06DA9040I, 05P12RDFN8, and 05P15RDFN1), the European Commission within the Seventh Framework Program through IA-ENSAR (Contract No. RII3-CT-2010-262010), the Hungarian OTKA Foundation No. K106035, the Sumitomo Foundation, the National Natural Science Foundation of China (Contract No. 11575269), the Helmholtz Association of German Research Centres through the Helmholtz-CAS Joint Research Group HCJRG-108, HIC for FAIR, GSI-RUG/KVI collaboration agreement, TU Darmstadt-GSI cooperation contract, and the STIBET Doctoral program of the German Academic Exchange Service.

[1] E. Rutherford, Philos. Mag. **21**, 669 (1911).
[2] R. Hofstadter, Rev. Mod. Phys. **28**, 214 (1956).
[3] I. Brissaud *et al.*, Nucl. Phys. A **191**, 145 (1972).
[4] G. D. Alkhazov *et al.*, Phys. Rep. **42**, 89 (1978).
[5] G. Alkhazov *et al.*, Nucl. Phys. A **712**, 269 (2002).
[6] P. Egelhof *et al.*, Eur. Phys. J. A **15**, 27 (2002).
[7] A. Dobrovolsky *et al.*, Nucl. Phys. A **766**, 1 (2006).
[8] S. Ilieva *et al.*, Nucl. Phys. A **875**, 8 (2012).
[9] A. Sedrakian, Prog. Part. Nucl. Phys. **58**, 168 (2007).
[10] B. A. Brown, Phys. Rev. Lett. **85**, 5296 (2000).
[11] H. H. Gutbrod *et al.*, FAIR Baseline Technical Report, ISBN 3-9811298-0-6 (2006).
[12] O. A. Kiselev, Phys. Scr. **T166**, 014004 (2015).
[13] B. Franzke, Nucl. Instrum. Meth. Phys. Res. B **24**, 18 (1987).
[14] M. von Schmid *et al.*, Nature (to be published).
[15] J. C. Zamora *et al.*, Phys. Lett. B **763**, 16 (2016).
[16] M. Steck *et al.*, Nucl. Instrum. Meth. Phys. Res. A **532**, 357 (2004).
[17] A. Gruber *et al.*, Nucl. Instrum. Meth. Phys. Res. A **282**, 87 (1989).
[18] M. Kühnel *et al.*, Nucl. Instrum. Meth. Phys. Res. A **602**, 311 (2009).
[19] M. Mutterer *et al.*, Phys. Scr. **T166**, 014053 (2015).
[20] B. Streicher *et al.*, Nucl. Instrum. Meth. Phys. Res. A **654**, 604 (2011).
[21] S. Agostinelli *et al.*, Nucl. Instrum. Meth. Phys. Res. A **506**, 250 (2003).
[22] J. C. Zamora, Nuclear Reaction Studies Using Stored Ion Beams at ESR with EXL, Ph.D. thesis, TU Darmstadt (2015).
[23] G. R. Satchler and D. T. Khoa, Phys. Rev. C **55**, 285 (1997).
[24] Y. W. Lui, D. H. Youngblood, H. L. Clark, Y. Tokimoto, and B. John, Phys. Rev. C **73**, 014314 (2006).
[25] I. J. Thompson, Computer code FRESCO, http://www.fresco.org.uk/.
[26] A. Kobos *et al.*, Nucl. Phys. A **425**, 205 (1984).
[27] D. T. Khoa and W. von Oertzen, Phys. Lett. B **342**, 6 (1995).
[28] P. J. Karol, Phys. Rev. C **11**, 1203 (1975).
[29] N. Takigawa *et al.*, Phys. Lett. B **288**, 244 (1992).
[30] L. Chulkov *et al.*, Nucl. Phys. A **603**, 219 (1996).
[31] M. S. Hussein, R. A. Rego, and C. A. Bertulani, Phys. Rep. **201**, 279 (1991).
[32] A. Ozawa *et al.*, Nucl. Phys. A **608**, 63 (1996).
[33] L. Ray, Phys. Rev. C **20**, 1857 (1979).
[34] A. Vitturi and F. Zardi, Phys. Rev. C **36**, 1404 (1987).
[35] H. D. Vries, C. D. Jager, and C. D. Vries, At. Data Nucl. Data Tables **36**, 495 (1987).
[36] C. Bertulani *et al.*, Comput. Phys. Commun. **152**, 317 (2003).
[37] G. Cowan, *Statistical Data Analysis*, Oxford Science Publications (Clarendon Press, Oxford, 1998).
[38] G. Alkhazov *et al.*, Phys. Lett. B **67**, 402 (1977).
[39] J. J. Kelly, Phys. Rev. C **66**, 065203 (2002).
[40] J. J. Kelly, Phys. Rev. C **70**, 068202 (2004).
[41] G. Colò *et al.*, Comput. Phys. Commun. **184**, 142 (2013).
[42] P. G. Reinhard, D. J. Dean, W. Nazarewicz, J. Dobaczewski, J. A. Maruhn, and M. R. Strayer, Phys. Rev. C **60**, 014316 (1999).
[43] L. Ray, W. R. Coker, and G. W. Hoffmann, Phys. Rev. C **18**, 2641 (1978).
[44] S. Terashima, H. Sakaguchi, H. Takeda, T. Ishikawa, M. Itoh, T. Kawabata, T. Murakami, M. Uchida, Y. Yasuda, M. Yosoi, J. Zenihiro, H. P. Yoshida, T. Noro, T. Ishida, S. Asaji, and T. Yonemura, Phys. Rev. C **77**, 024317 (2008).